

Original Article

Identifying absorbable bioactive constituents of Yupingfeng Powder acting on COVID-19 through integration of UPLC-Q/TOF-MS and network pharmacology analysis

Linyan Wang^{a,*}, Zhongyan Du^a, Yang Guan^a, Bo Wang^a, Yanling Pei^b, Lizong Zhang^a, Mingsun Fang^a

^aAcademy of Chinese Medical Sciences, Zhejiang Chinese Medical University, Hangzhou 310053, China

^bXinminhe Pharmaceutical Research & Development (HeBei) Co., Ltd., Baoding 071200, China

ARTICLE INFO

Article history:

Received 24 February 2021

Revised 15 April 2021

Accepted 8 July 2021

Available online 9 February 2022

Keywords:

COVID-19
network pharmacology
UPLC-Q/TOF-MS
Yupingfeng Powder

ABSTRACT

Objective: Yupingfeng Powder (YPF), a kind of preventative patent medicine, is chosen for treatment of coronavirus disease 2019 (COVID-19) due to its high frequency application in respiratory tract diseases, such as chronic obstructive pulmonary disease, asthma, respiratory tract infections, and pneumonia, with the advantage of reducing the relapse rate and the severity. However, the active components of YPF and the mechanisms of components affecting COVID-19 are unclear. This study aimed to determine active constituents and elucidate its potential mechanisms.

Methods: Ultra performance liquid chromatography–quadrupole–time of flight mass spectrometry (UPLC-Q/TOF-MS) and liquid chromatography–triple quadrupole mass spectrometry (LC-QQQ-MS) were used to determine the components and absorbable constituents of YPF. Secondly, TCMSP, Drugbank, Swiss and PharmMapper were used to search the targets of absorbable constituents of YPF, and the targets of COVID-19 were identified based on GeneCards and OMIM databases. STRING database was used to filter the possible inter-protein interactions. Thirdly, Gene Ontology (GO) enrichment analysis and Kyoto Encyclopedia of Genes and Genomes (KEGG) pathways analysis were performed to identify molecular function and systemic involvement of target genes.

Results: A total of 61 components of YPF and 36 absorbable constituents were identified through UPLC-Q/TOF-MS. Wogonin, prim-O-glucosylcimifugin, 5-O-methylvisamminol, astragaloside IV and 5-O-methylvisamminol (hydroxylation) were vital constituents for the treatment of COVID-19, and RELA, TNF, IL-6, MAPK14 and MAPK8 were recognized as key targets of YPF. The major metabolic reactions of the absorbed constituents of YPF were demethylation, hydroxylation, sulfation and glucuronidation. GO and KEGG pathway analysis further showed that the most important functions of YPF were T cell activation, response to molecule of bacterial origin, cytokine receptor binding, receptor ligand activity, cytokine activity, IL-17 signaling pathway, Chagas disease, lipid and atherosclerosis, etc.

Conclusion: The approach of combining UPLC-Q/TOF-MS with network pharmacology is an effective tool to identify potentially bioactive constituents of YPF and its key targets on treatment of COVID-19.

© 2022 Tianjin Press of Chinese Herbal Medicines. Published by ELSEVIER B.V. This is an open access article under the CC BY-NC-ND license (<http://creativecommons.org/licenses/by-nc-nd/4.0/>).

1. Introduction

Corona Virus Disease 2019 (COVID-19), which is caused by a newly identified coronavirus Severe Acute Respiratory Syndrome Coronavirus 2 (SARS-CoV-2), has spread to about 215 countries and regions around the world, with about seven million confirmed cases, endangering the health of people all over the world and causing a global health crisis. In the theory of traditional Chinese medicine (TCM), 2019-new coronavirus (2019-nCoV) infected

pneumonia was deemed to the category of “Pestilence”, and the characteristic of its pathogenesis was “dampness, toxin, stasis and closure”, which consumes *Qi* and *Yin* and leads to a deficiency (Chen, Wang, Shi, & Fang, 2020; Wang et al., 2020; You, Yan, Wang, Luo, & Zhao, 2020; Zhang et al., 2020). Chinese medicine had been used to treat and prevent viral infection pneumonia diseases for thousands of years and had accumulated a large number of clinical experience and effective prescriptions (Luo et al., 2020). As recommended in the *Guideline on Diagnosis and Treatment of Coronavirus Disease 2019* (Revised 7th version), which was officially released by National Health Commission of the People’s Republic of China, TCM had achieved good clinical effects in treatment of COVID-19,

* Corresponding author.

E-mail address: linyan0520@126.com (L.y. Wang).

because of its unique therapeutic principles including syndrome differentiation and treatment, boosting the individual's endogenous healing ability, balancing *Yin* and *Yang* (Du, Hou, Miao, Huang, & Liu, 2020; Yang, Islam, Wang, Li, & Chen, 2020).

Yupingfeng Powder (YPF), a kind of preventative patent medicine, is chosen (Xu & Zhang, 2020) due to its high frequency application in respiratory tract diseases, such as chronic obstructive pulmonary disease (Ma et al., 2018), asthma (Liu et al., 2017; Wang et al., 2016), respiratory tract infections (Song et al., 2016), and pneumonia (Yan et al., 2010), with the advantage of reducing the relapse rate and the severity. Its recipe contains three herbal medicines including *Astragali Radix*, *Atractylodis Macrocephalae Rhizoma* and *Saposhnikoviae Radix*. In which, *Astragali Radix* acts as the monarch herb due to the flavonoids and saponins have the effects of boosting energy, strengthening the immune system, and promoting healthy activities (Oh, Choi, Kim, & Kim, 2014; Shi et al., 2015). The main constituents in *Saposhnikoviae Radix* are chromones and coumarins, such as cimifugin, prim-*O*-glucosylcimifugin, *sec-O*-glucosylhamaudol and so on, which concentrate in the antipyretic, analgesic, anti-inflammatory effects (Han et al., 2016; Nikles et al., 2017; Yang et al., 2017); And the major bioactive constituents in *Atractylodis Macrocephalae Rhizoma* are amino acids, polysaccharides and lactones which show anti-inflammatory and immune regulation (Sun et al., 2015; Zhao et al., 2016). Recently, many researchers poured attention into the pharmacology and pharmacological mechanisms of YPF acting on respiratory tract diseases (Li et al., 2014; Li et al., 2017) integrated with network pharmacology (Shen, Chen, Zhang, Liu, & Cao, 2019; Zuo et al., 2018). However, the studies gathering compounds from various databases to generate compound-target maps may produce false-positive results, for some substances with plenty of targets but possess low bioavailability are also taken into account. In this context, we focused on the absorbable constituents as selected target constituents, then integrated the target constituents and corresponding target proteins by network pharmacology. The absorbed substances were identified by UPLC-Q/TOF-MS method, and a network pharmacology investigation was conducted to determine the potential key constituents and targets (Fig. 1).

2. Materials and methods

2.1. Materials

Astragali Radix, *Atractylodis Macrocephalae Rhizoma* and *Saposhnikoviae Radix* were purchased from Binjiang Chinese Medicine Clinic of Zhejiang Chinese Medical University. All the botanical characters of the herbs were identified by associate professor Feiye Zhu (Zhejiang Chinese Medical University). Acetonitrile, methanol, and formic acid (HPLC-grade) were obtained from Merck (Darmstadt, Germany). The distilled water was prepared by a Milli-Q (Milford, MA, USA). Leucine enkephalin and sodium formate were obtained by Waters (Milford, USA). All the chemicals met the analytical or higher grade. Cimifugin, *sec-O*-glucosylhamaudol, atractylenolide I, atractylenolide II, calycosin and wogonin were purchased from Shanghai Nature Standard Technology Co., Ltd. (Shanghai, China). Formononetin and 5-*O*-methylvisammoside were purchased from Chengdu Pufei De Biotech Co., Ltd. (Chengdu, China). Prim-*O*-glucosylcimifugin, astragaloside IV and atractylenolide III were purchased from National Institutes for Food and Drug Control Pharmaceutical and Biological Products (Beijing, China).

2.2. Extractions

YPF composes of *Astragali Radix*, *Atractylodis Macrocephalae Rhizoma* and *Saposhnikoviae Radix* in a dry weight ratio of 2:2:1. The pieces (150 g) were weighed and double extracted by refluxing with boiling water (1:10, mass to volume ratio) for 1.5 h. Thereafter the water decoction was concentrated to 1.0 g/mL (crude drugs) and centrifuged at 12000 rpm for 15 min, and the supernatant was stored at 4 °C before analysis.

2.3. Animal preparation

Six male Wistar rats (200–220 g) were applied in the study. Rats were obtained from Laboratory Animal Research Center of Zhejiang Chinese Medical University (Hangzhou, China). All experimental protocols were in accordance with the guidelines approved by

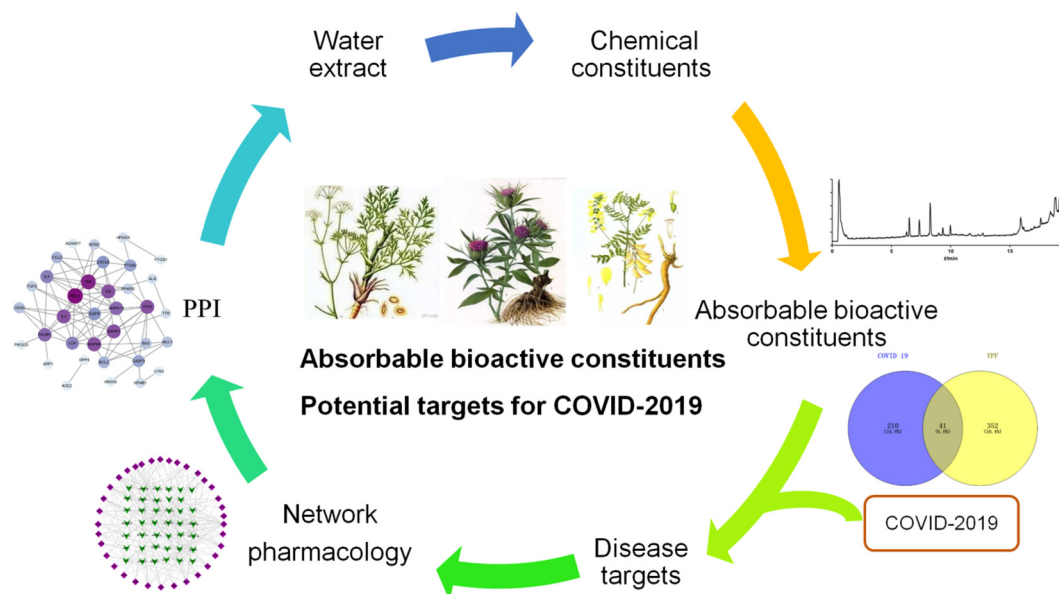


Fig. 1. Process for identifying potential active components and targets of YPF extracts with activity against COVID-19 through integrated UPLC-Q/TOF-MS and network pharmacology.

The Animal Ethical Committee of Zhejiang Chinese Medical University (approval number: SYXK(Zhe) 2018-0012).

2.4. Serum collection and preparation

Before the day of last administration, the rats were fasted for 12 h but allowed water. Six rats were intragastrically administered with YPF (12 g/kg). Blood samples were collected in heparinized tubes via the orbital venous plexus from each rat before drug administration and at 10, 20, 40, 60 min after drug administration. Pharmacokinetics studies have proved that the peak time (T_{max}) of flavonoids after oral administration of *Astragali Radix* were ranged from 10.8 min to 50.0 min (Shi et al., 2015), the main components of T_{max} of *Saposhnikovia Radix* were ranged from 12.0 min to 70 min (Jia, Xiong, Xue, Wang, & Yan, 2017; Li et al., 2012). Based on above parameters, 10, 20, 40, 60 min were chosen as four time points to obtain the dosed plasma and mixed for later analysis. The blood samples were then immediately centrifuged at 5000 rpm for 5 min to collect the plasma and the plasma of different time points were mixed. The plasma (100 μ L) was mixed with 400 μ L of methanol at 4 °C, vortexed 1 min and centrifuged at 13,500 rpm for 10 min. The supernatant was dried with nitrogen gas at 40 °C, added 100 μ L 50% methanol to reconstitute the residue, centrifuged at 12,000 rpm for 15 min, transferred to a vial and injected 2 μ L and 5 μ L for UPLC-Q/TOF-MS analysis and liquid chromatography-triple quadrupole mass spectrometry (LC-QQQ-MS) analysis, respectively.

2.5. Chromatographic and mass spectrometric conditions

The electrospray ionization (ESI) was used as the ionization source by Q-TOF SYNAPT G2-Si High Definition Mass Spectrometer (Waters, UK). The separation was performed by a Waters ACQUITY UPLC BEH C₁₈ Column (2.1 \times 50 mm, 1.7 μ m) with BEH C₁₈ Van Guard (2.1 mm \times 50 mm, 1.7 μ m) at 40 °C. Briefly, in ESI-MS analysis, the capillary voltage was set as 3.0 kV. The MS^E continuum mode was carried out over the range of m/z 50–1200. Each sample was injected 2 μ L into the column and employed with a gradient elution. The column and autosampler temperature were maintained at 40 °C and 4 °C. The gradient elution consisted of A (methanol) and B (0.1% formic acid in water), the flow rate was controlled at 0.25 mL/min. The gradient program was set as follows: 0–0.5 min, 5% A; 0.8–10 min, 5%–55% A; 10–15 min, 55%–70% A; 15–19 min, 70%–95% A; 19–20 min, 95% A.

The LC-QQQ-MS procedure was performed by using SHIMADZU LC-20A system and SHIMADZU 8050 Triple Quadrupole mass spectrometer equipped with an ESI source. Chromatographic separation was achieved on an InertSustain C₁₈ column (4.6 mm \times 150 mm, 5 μ m) at 40 °C. The mobile phases consisted of A (methanol) and B (0.1% formic acid in water). The gradient program was set as follows: 0–0.5 min, 5% A; 0.5–7 min, 5%–40% A; 7–30 min, 40%–85% A; 30–35 min, 85%–95% A; 35–38 min, 95% A; The flow rate was 0.6 mL/min, and the injection volume was 5 μ L. The mass spectrometer was operated in positive ion mode.

Table 1
LC-MS characteristics of four standards.

Components	Precursor ion (m/z)	Product ion (m/z)	Collision energy (eV)
Formononetin	269.05	197.05	39
Calysion	285.05	253.05	26
Astragaloside IV	807.45	627.20	24
Atractylenolide II	233.10	187.10	13

Analysis was performed by multiple reactions monitoring (MRM), the parameters were summarized in Table 1.

2.6. Network pharmacology

2.6.1. Compound targets of YPF

As the absorbed constituents were more probably the bioactive compounds, the prototype components and metabolites identified by UPLC-Q/TOF-MS were used to construct the chemical information database of YPF for network pharmacology research. The targets of prototype components and metabolites were collected from TCMSP (<http://tcmssp.com/tcmssp.php>) (Ru et al., 2014), Drugbank (<https://www.drugbank.ca/>), Swiss (<http://www.swisstargetprediction.ch/>) (Gfeller, Michielin, & Zoete, 2013) and PharmMapper (<http://www.ililab-ecust.cn/pharmmapper/>) (Liu et al., 2010; Wang, Pan, Gong, Liu, & Li, 2016; Wang et al., 2017). The molecular files of the prototype compounds were downloaded from PubChem (<https://pubchem.ncbi.nlm.nih.gov/>) and the metabolites were drawn by Chem3D. All the structures were saved in sdf format. Then the targets of these compounds were obtained from PharmMapper. To improve the reliability of the target prediction results, the top 30 matches (Z -Score > 0.3).

2.6.2. Protein-protein interactions (PPIs)

STRING database (<http://string-db.org/>) was used to filter the possible inter-protein interactions (PPIs) (Von Mering et al., 2003). The attained PPIs with high confidence (combine score > 0.90) were kept for network construction and analysis.

2.6.3. Network construction and analysis

Cytoscape software (version 3.7.1) was applied to create a network compounds-target network and PPIs network. The parameters of average shortest pathway length (ASPL) and betweenness centrality (BC) were calculated by Network Analyzer (Arrell, Zlatkovic, Kane, Yamada, & Terzic, 2009). To identify the hub targets, Cytoscape was applied to further analyze the PPIs network (Zhai et al., 2020).

2.6.4. Construction of target gene network

Gene Ontology (GO) enrichment analysis and Kyoto Encyclopedia of Genes and Genomes (KEGG) pathways analysis were performed to identify molecular function and systemic involvement of target genes. GO classification and enrichment analysis of potential target genes were performed using the STRING database (<https://string-db.org/>). The top 10 results of molecular function, biological process, and cell component analysis were selected, and R software (R version 3.6.0) was used for plotting. The top 10 pathway information was selected with P less than 0.05, Omicshare database (<http://www.omicshare.com>), and the histogram was drawn using R software.

3. Results

3.1. Identification of YPF components

In total, 61 compounds in YPF were successfully characterized through comparison with the UNIFI software (version 1.7) and literatures. Eleven of these compounds were further confirmed by the reference standards. All YPF component information was summarized in Table S1. The total ion chromatograms of YPF extracts obtained in positive and negative modes were shown in Fig. S1. Diverse components, seven amino acids, 14 chromogens, 13 flavonoids, 14 saponins, 11 lactones and two others were identified in YPF. Among these components, chromogens, flavonoids and saponins were the major components of YPF. By analyzing their struc-

tural features, fragmentation patterns, and typical peak ions in MS^e high spectra, the components and their fragmentation patterns were identified. It could be summarized as follows and some specific compounds were taken as examples.

3.1.1. Flavonoids

Thirteen flavonoids mainly originated from *Astragali Radix*, including calycosin, formononetin, calycosin-7-*O*- β -*D*-glucoside, ononin and methylnissoin-3-*O*-glucoside. Flavonoids often lose neutral fragments of CO, H₂O, CHO and methyl radical (containing methoxy group), and also undergo RDA cleavage to form fragmented ions, while flavonoid glycosides often remove glycosyl groups in mass spectrometry. The molecular formula of compound **23** was C₂₂H₂₂O₉ provided by LC-Q/TOF-MS. It generated adduct ion [M + H]⁺ at *m/z* 431.1342 and base peak ion at *m/z* 269 [M + H-C₆H₁₀O₅]⁺ in MS^e high spectrum, indicating the existence of glucose. It exhibited molecule at *m/z* = 254[M + H-C₆H₁₀O₅-CH₃]⁺, *m/z* = 226[M + H-C₆H₁₀O₅-CH₃-CO]⁺ and *m/z* = 225[M + H-C₆H₁₀O₅-CH₃-CHO]⁺. *m/z* = 137[M + H-C₉H₈O]⁺ and *m/z* = 118[M + H-C₇H₆O₃-CH₃]⁺ showed RDA fragmentation occurring. Compared with reference of formononetin, compound **23** was proposed to be ononin. Its proposed fragmentation patterns were shown in Fig. 2.

3.1.2. Chromones

Chromones are the main active components of *Saposhnikovia Radix*, and divided into three categories: furanochromone, pyranochromone and others. Cimifugin, prim-*O*-glucosylcimifugin, 5-*O*-methylvisammioside and 5-*O*-methylvisammimol belong to furanochromone while *sec-O*-glucosylhamaudol and hamaudol are classed as pyranochromone. Compound **24** had molecular formula C₂₂H₂₈O₁₀, as well as base peak ions at *m/z* = 291[M + H-C₆H₁₀O₅]⁺ in its MS^e high energy mode. Besides, it generated fragment ions at *m/z* = 273[M + H-C₆H₁₀O₅-H₂O]⁺ by partly losing H₂O. The fragment ions at *m/z* = 243 and *m/z* = 216 corresponded with [M + H-C₆H₁₀O₅-H₂O-2CH₃]⁺ and [M + H-C₆H₁₀O₅-H₂O-C₄H₉]⁺. *m/z* = 219[M + H-C₆H₁₀O₅-C₄H₈O]⁺ showed RDA fragmentation

occurring. Therefore, it was supposed as 5-*O*-methylvisammioside (Fig. 3).

3.2. Characterization of absorbed prototype constituents

To characterize the absorbable constituents of YPF, a UPLC-Q/TOF-MS method with UNIFI software was utilized to screen the constituents. The absorbed constituents were shown in Table 2, and a total of nine prototype constituents were found in the dosed plasma. Of note, the mass errors of the identified constituents were less than 10×10^{-6} , and the numbers of constituents identified from *Astragali Radix* and *Saposhnikovia Radix* were one and eight, respectively. The vast majority of prototype constituents were chromones of *Saposhnikovia Radix*. Based on this situation, and according to the literatures, MRM mode of LC-QQQ-MS with high sensitivity was utilized. Calycosin, formononetin, atractylenolide II and astragaloside IV were detected by MRM mode (Fig. 4). Totally, the numbers of prototype constituents identified from *Astragali Radix*, *Atractylodis Macrocephalae Rhizoma* and *Saposhnikovia Radix* were four, one and eight. The MS spectrums were shown as supplement Figs. S2–S10.

3.3. Identification of metabolites and possible metabolic routes

The peaks detectable in dosed rat plasma and not in blank rat plasma were considered as probable metabolites. The metabolites of the absorbed substances in rat plasma were further analyzed by UNIFI software. Furthermore, the ion of MS^e high energy mode was analyzed to further identify the structures. Finally, a total of 23 metabolites were observed (Table 3). The MS spectrums were shown as supplement Figs. S11–S33.

Flavonoids, major constituents originated from *Astragali Radix*, might be undergoing hydroxylation, dehydroxylation, glucuronide conjugation or sulfate conjugation after oral administration in phase I/II reactions. As shown in Fig. 5, the metabolic pathways of some major flavonoids after oral administration of YPF were proposed. The biotransformation between the main flavonoids and their glucuronides could be a fundamental factor of the phar-

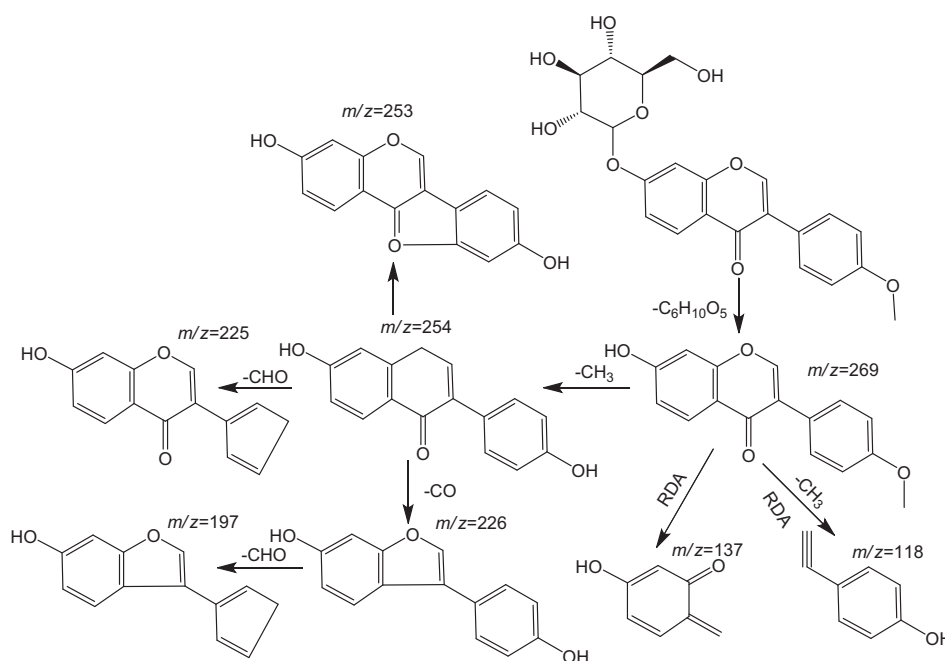


Fig. 2. Proposed fragmentation patterns of ononin.

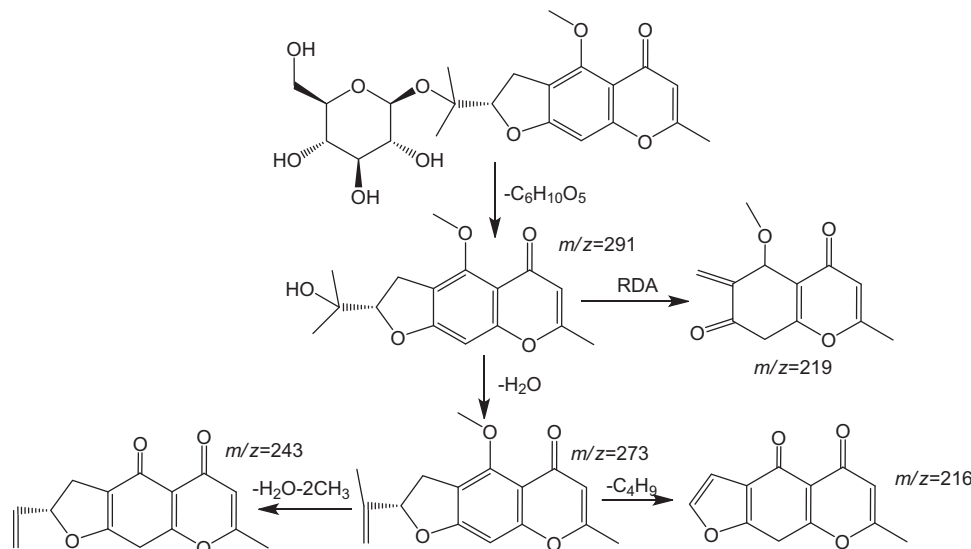


Fig. 3. Proposed fragmentation patterns of 5-O-methylvisammioside.

Table 2
Characterization of prototype constituents in dosed plasma by UPLC-Q/TOF-MS.

No.	t_R (min)	Element composition	Ion mode	m/z	Observed m/z	Error ($\times 10^{-6}$)	Fragment ions	Compounds	Sources
P1	6.51	$C_{22}H_{28}O_{11}$	+	469.1710	469.1710	0.0	307, 289, 259, 235, 221	prim-O-glucosylcimifugin ^a	<i>Saposhnikovia Radix</i>
P2	7.38	$C_{16}H_{18}O_6$	+	307.1182	307.1181	-0.3	259, 235, 221, 177	cimifugin ^a	<i>Saposhnikovia Radix</i>
P3	7.54	$C_{16}H_{12}O_5$	+	285.0765	285.0763	-0.7	270, 253	wogonin ^a	<i>Saposhnikovia Radix</i>
P4	8.25	$C_{22}H_{22}O_9$	+	431.1342	431.1342	0.0	269, 254	ononin	<i>Astragali Radix</i>
P5	8.28	$C_{22}H_{28}O_{10}$	+	453.1752	453.1748	-0.9	291, 273	5-O-methylvisammioside ^a	<i>Saposhnikovia Radix</i>
P6	8.84	$C_{15}H_{16}O_6$	+	293.1017	293.1025	2.7	221, 275, 233	3S-2,2-dimethyl-3,5-dihydroxy-8hydroxymethyl-3,4-dihydro-2H,6H-Benz[1,2-b:5,4-b']Dipyran-6-one	<i>Saposhnikovia Radix</i>
P7	9.37	$C_{16}H_{18}O_5$	+	291.1227	291.1236	3.1	273, 243, 219	5-O-Methylvisammioside	<i>Saposhnikovia Radix</i>
P8	9.97	$C_{21}H_{26}O_{10}$	+	439.1601	439.1599	-0.5	277, 259, 205, 217, 189	sec-O-glucosylhamaudol ^a	<i>Saposhnikovia Radix</i>
P9	11.00	$C_{15}H_{16}O_5$	+	277.1076	277.1075	-0.4	259, 205, 217	hamaudol	<i>Saposhnikovia Radix</i>

a: Compounds were compared with reference standards.

macological effects of *Astragali Radix* (Shi et al., 2015). M8 $[M + H]^+$ ions at m/z 461.1077, which corresponded with the formula of $C_{22}H_{20}O_{11}$. It was apt to experience the neutral loss of 176 Da ($C_6H_8O_6$), and yielded product ions at m/z 285, 270, 253 and 225 in MS^E spectrum. We presumed that it might be the glucuronide conjugates of calycosin at C7 or C3' positions. However, the position of glucuronide conjugates could hardly be located, due to the same product ions in MS^E spectrum. M10 and M11, the components metabolized from formononetin phase II reactions, were tentatively characterized as the glucuronide and sulfate conjugated metabolites, respectively. Moreover, M9 metabolized from formononetin through both of phase I and phase II reactions, was tentatively characterized as the successive hydroxyl and glucuronide conjugated metabolites.

A total of nine phase I metabolites, mainly hydroxylation and demethylation and six phase II metabolites of chromones were matched by UNIFI software and then identified in rat plasma after oral administration of YPF. The structures were proposed on the basis of the characteristics of their precursor ions, MS^E product ions and chromatography retention times. The characteristic fragment

ions of cimifugin (P2) at m/z 259 and 235 in positive ion mode could be observed in the MS^E profile of M1, M3, M4 and M5. M1 and M4 exhibited the $[M + H]^+$ ion at m/z 323.1130, which were 16 Da higher than the ion of P2, indicating the hydroxylation might be taken place. The fragment ions of M5 at m/z 307 were formed by loss of $C_6H_8O_6$ (176 Da) from the $[M + H]^+$ ion, thus, it was designated as glucuronide conjugate P2. Conjugation with sulfate group was also the major phase II reaction of P2. For example, M3 showed the $[M + H]^+$ ions at m/z 385.0595 (the formula of $C_{16}H_{18}O_9S$, mass error within 0.3×10^{-6}). Other metabolic reactions for P2 included demethylation. For example, M6 was 14 Da lower than the ion of P2, indicating the molecular formula of $C_{15}H_{16}O_6$. The proposed metabolic pathways of cimifugin were shown in Fig. 6 based on the presence of diagnostic ions and the data of literature.

3.4. Target network pharmacological analysis of bioactive constituents

3.4.1. Absorbed constituents with related target proteins

By searching TCMS Database, PharmMapper, Drugbank Database and Swiss Database, a total of 394 putative targets

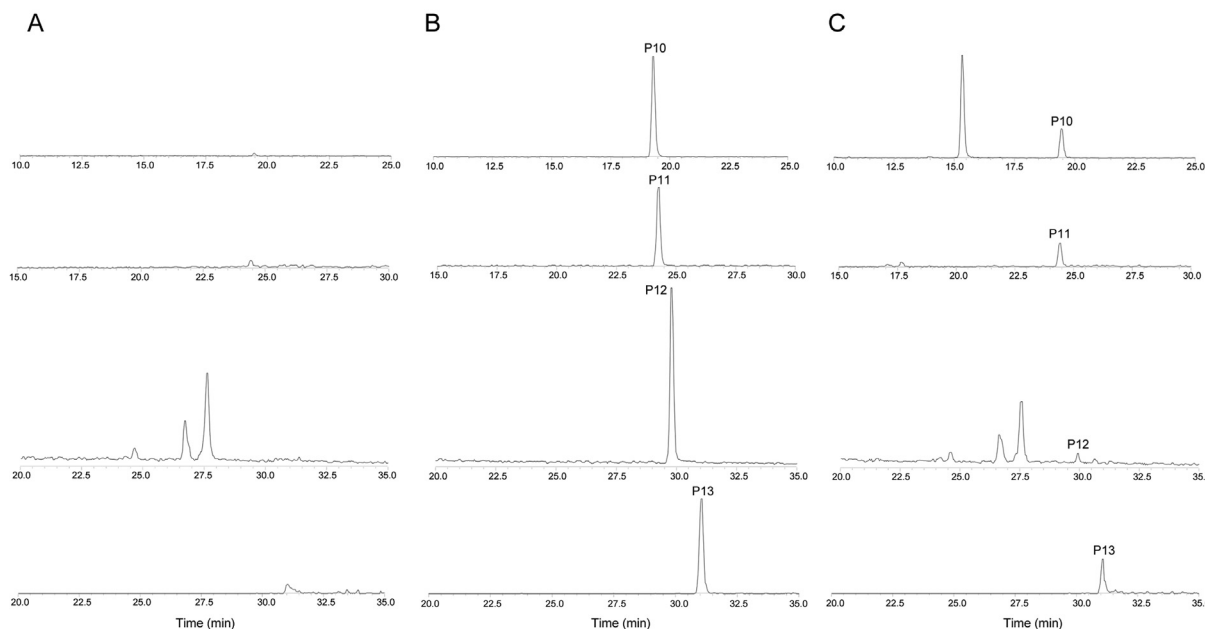


Fig. 4. Representative MRM chromatograms of (A) blank plasma, (B) reference standards and (C) plasma samples after oral administration of YPF. Calycosin (P10): 19.301 min; formononetin (P11): 24.262 min; atractylenolide II (P12): 29.793 min; astragaloside IV (P13): 31.058 min.

Table 3
Characterization of metabolites in dosed plasma by UPLC-Q/TOF-MS.

Compounds	No.	t _R (min)	Element composition	Ion mode	m/z	Observed m/z	Error (×10 ⁻⁶)	Fragment ions	Metabolic pathways
Cimifugin	M1	5.09	C ₁₆ H ₁₈ O ₇	+	323.1130	323.1118	-3.7	235, 259, 221	hydroxylation
	M2	5.44	C ₁₆ H ₁₈ O ₇	+	323.1130	323.1131	0.3	232, 247	hydroxylation
	M3	6.28	C ₁₆ H ₁₈ O ₉ S	-	385.0594	385.0591	-0.8	177	sulfate conjugation
	M4	6.33	C ₁₆ H ₁₈ O ₇	+	323.1130	323.1125	-1.5	235, 221	hydroxylation
	M5	6.47	C ₂₂ H ₂₆ O ₁₂	+	483.1502	483.1503	0.2	307, 289, 259, 235	glucuronide conjugation
Calycosin-7-O-β-D-glucoside	M6	8.63	C ₁₅ H ₁₆ O ₆	+	293.1017	293.1022	1.7	221, 275	demethylation
	M7	5.28	C ₂₈ H ₃₀ O ₁₆	+	623.1612	623.1594	-2.9	447, 285, 270	glucuronide conjugation
Calycosin	M8	7.53	C ₂₂ H ₂₀ O ₁₁	+	461.1084	461.1077	-1.5	285, 270, 253, 225	glucuronide conjugation
Formononetin	M9	7.54	C ₂₂ H ₂₀ O ₁₁	-	459.0927	459.0929	0.4	283	hydroxylation + glucuronide conjugation
	M10	8.10	C ₂₂ H ₂₀ O ₁₀	+	445.1135	445.1131	-0.9	269, 254	glucuronide conjugation
Isomucronulatol	M11	8.65	C ₁₆ H ₁₂ O ₇ S	-	347.0225	347.0226	0.3	267, 252, 208	sulfate conjugation
	M12	6.63	C ₁₇ H ₁₈ O ₉ S	-	397.0593	397.0591	-0.5	317	hydroxylation + sulfate conjugation
Isomucronulatol-7-O-β-D-glucoside	M13	9.27	C ₂₃ H ₂₆ O ₁₁	-	477.1397	477.1397	0.0	301, 286	glucuronide conjugation
	M14	7.92	C ₂₉ H ₃₆ O ₁₆	-	639.1925	639.1924	-0.2	463, 301, 121	glucuronide conjugation
Methylnissolin	M15	8.32	C ₂₃ H ₂₄ O ₁₁	+	477.1397	477.1389	-1.7	301, 167, 152	glucuronide conjugation
5-O-methylvisamminol	M16	6.36	C ₁₅ H ₁₆ O ₅	-	275.0920	275.0912	-2.9	260	demethylation
	M17	8.22	C ₁₆ H ₁₈ O ₆	+	307.1184	307.1179	-1.6	216, 259, 231	hydroxylation
Hamaudol	M18	8.95	C ₁₆ H ₁₈ O ₆	+	307.1184	307.1156	-9.1	259, 235, 231	hydroxylation
	M19	8.34	C ₂₂ H ₂₆ O ₁₁	+	467.1553	467.1550	-0.6	291, 273	glucuronide conjugation
	M20	8.63	C ₁₅ H ₁₆ O ₆	+	293.1025	293.1024	-0.3	275, 221	hydroxylation
	M21	8.12	C ₂₁ H ₂₄ O ₁₂	+	469.1346	469.1350	0.9	293, 275	Hydroxylation + glucuronide conjugation
	M22	9.32	C ₁₄ H ₁₄ O ₅	+	263.0919	263.0905	-5.3	217, 189	demethylation
	M23	10.11	C ₂₁ H ₂₄ O ₁₁	+	453.1397	453.1405	1.8	277, 259	glucuronide conjugation

of the YPF absorbed constituents were screened in the database, and visualized in Fig. S34. These networks are involved mainly in cancer, diabetes, osteopetrosis, cell death and survival, chronic obstructive pulmonary disease, estrogen resistance, as well as inflammatory responses. TTR, MAPK14 and PPARγ, the target genes of COVID-19, make interaction with 18 (P10, M8,

P11, M11, M14, M15, P13, P12, M1, M4, M6, M16, M17, M18, M20, M22, P6, M3) 17 (P10, P11, M11, M15, P13, M1, M2, M4, M6, M17, M18, M20, M22, M23, P6, P3, M3) and 17 (P10, M8, M7, P11, M11, P4, M12, P13, P12, M5, M17, M18, M20, M23, P6, P3, M3) absorbed constituents of YPF, respectively.

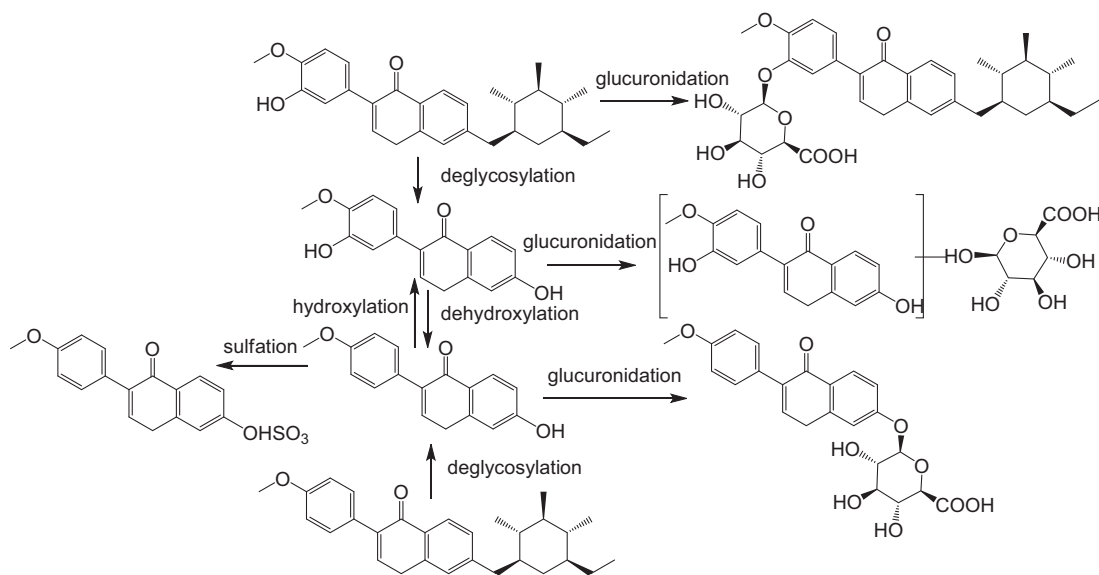


Fig. 5. Proposed pathways of metabolism and biotransformation of main flavonoids in YPF.

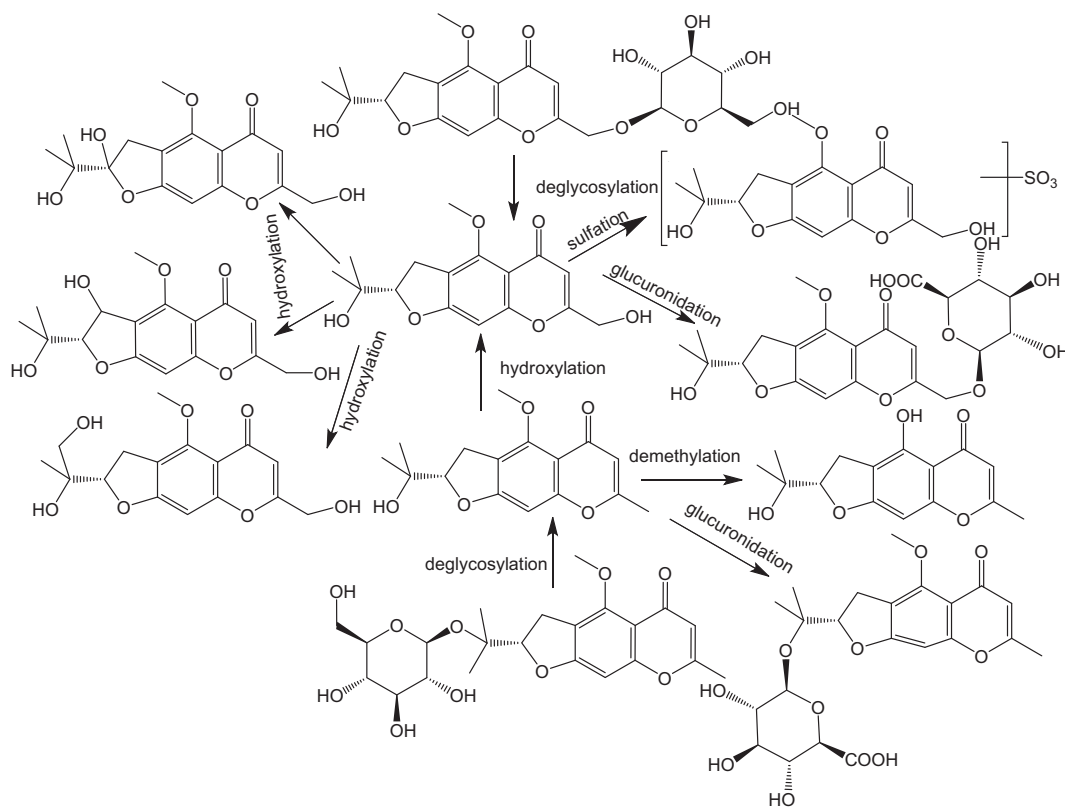


Fig. 6. Proposed pathways of metabolism and biotransformation of cimifugin in YPF.

3.4.2. Absorbed constituents target disease network

A total of 394 putative targets of the YPF components and 251 COVID-19 related targets were identified. Among all targets, 41 overlapped genes were identified, and were kept for network construction (Fig. 7). By operating network analyzer, topological parameters such as degree, ASPL and BC were attained (Table S2). The five components with largest BC and smallest ASPL were identified as the key components of YPF, including wogonin, prim-O-glucosylcimifugin, 5-O-methylvisamminol, astragaloside

IV and 5-O-methylvisamminol (hydroxylation) (Table 4). Among the five ingredients, wogonin was found with the smallest ASPL (2.38) and largest BC (0.27).

3.4.3. YPF PPIs network construction and topological analysis

Among the overlapped 41 targets, a total of 346 protein-protein interactions (PPIs) were obtained from STRING Database. By comparing the combine scores of the PPIs, 91 PPIs (P -value > 0.9, high confidence) were kept for PPIs network construction using Cytos-

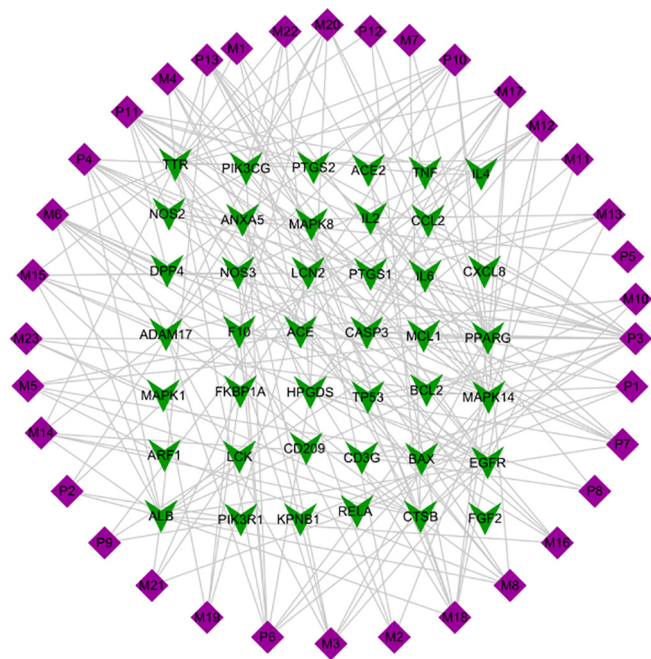


Fig. 7. Interaction network of targets of absorbed constituents and COVID-19. A node stands for constituents (in purple square) or target (in green arrow).

cape software (Fig. 8, Table S3). With the analysis using Cytohubba, RELA, TNF, IL-4, IL-6, CXCL8, IL-2, CCL2, MAPK14, MAPK8 and LCK were found with the highest average scores (Table 5-Cytohubba). Among the ten top ranked hub targets, RELA, TNF, IL-6, MAPK14 and MAPK8 were also recognized as key targets by network analyzer (Table 5-network analyzer), and therefore were identified as key targets for the treatment of COVID-19 of YPF. Among five key components of YPF, wogonin, astragaloside IV and 5-O-methylvisamminol (hydroxylation) interacted with four, two, and one hub targets respectively, were considered active constituents with activity against COVID-19 in this study. The details were summarized in Table 6.

3.4.4. Bioinformatics of COVID-19 targets of YPF

The results of GO and KEGG analysis were shown in Fig. 9. The T cell activation, response to lipopolysaccharide, response to molecule of bacterial origin, response to oxidative stress and positive regulation of establishment of protein localization ranked first in BP (Fig. 9A). Molecular functions of these proteins include cytokine receptor binding, phosphatase binding, receptor ligand activity, protein phosphatase binding and cytokine activity (Fig. 9B). Membrane raft, membrane microdomain, membrane region, vesicle lumen and secretory granule lumen were the top ones in CC (Fig. 9C). KEGG pathway analysis further showed that YPF targeted proteins are involved in IL-17 signaling pathway, AGE-RAGE signaling pathway in diabetic complications, Chagas disease, lipid and atherosclerosis and Kaposi sarcoma-associated herpesvirus infection (Fig. 9D).

Table 4
Results of network pharmacology analysis.

Components	Molecular names	Herbs	Average shortest pathlength	Betweenness centrality	Degree
P3	wogonin	<i>Saposhnikoviae Radix</i>	2.386667	0.274797	18
P7	5-O-Methylvisamminol	<i>Saposhnikoviae Radix</i>	2.653333	0.058268	5
P1	prim-O-glucosylcimifugin	<i>Saposhnikoviae Radix</i>	3.693333	0.053736	8
P13	astragaloside IV	<i>Astragali Radix</i>	2.493333	0.051852	8
M17	5-O-Methylvisamminol (hydroxylation)	<i>Saposhnikoviae Radix</i>	2.6	0.051665	8

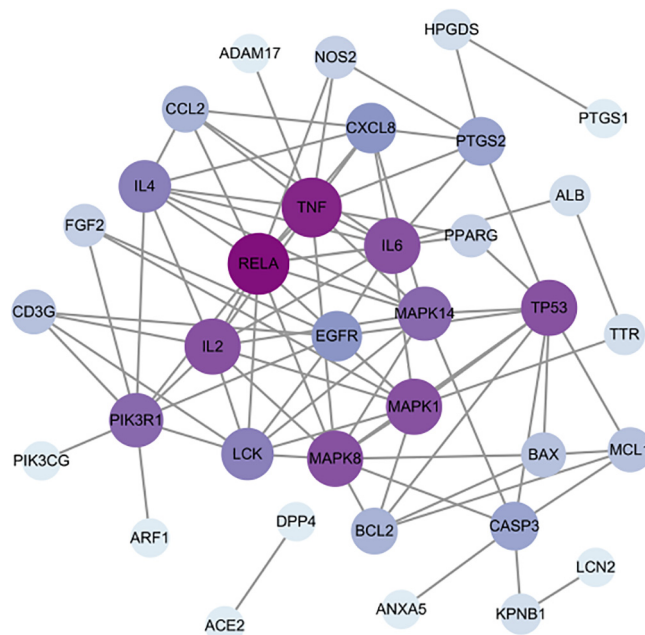


Fig. 8. Protein-protein interaction network.

4. Discussion

This study systematically explored the pharmacological mechanisms of YPF in the treatment of COVID-19 through UPLC-Q/TOF-MS and network pharmacology analysis. Network pharmacology can identify potentially active compounds, targets, and pharmacological mechanisms of complex compounds in Chinese herbal formulas (Li et al., 2020). However, the compounds of abundance of network pharmacology researches were collected from databases, which are related to plenty of targets but have lower bioavailability. Our study, which is constructed by the absorbable constituents and the corresponding targets, provided a better understanding of the metabolic and therapeutic pathways of TCM *in vivo*. For example, 5-O-methylvisamminol (3' hydroxylation), a metabolite of 5-O-methylvisamminol, played a vital role in the regulation of target of COVID-19, which could not be collected from databases directly. However, the research of the absorbed ingredients is based on the theory of that only some components absorbed in the body possess therapeutic effects, or produced from several reactions in the body ignoring components that play a regulatory role in intestinal flora to possess therapeutic effects, just like polysaccharides of YPF (Yin et al., 2019). So, we will explore the effect of YPF on intestinal flora in the future research.

Via network pharmacology analysis, three key active components were regarded to be effective on COVID-19, and five targets were screened to be effective on COVID-19. Multiple studies have indicated that two of these components are effective against COVID-19 (Huang, Bai, He, Xie, & Zhou, 2020; Ye et al., 2020). Wogonin, a flavonoid compound was considered to be the most

Table 5
Key targets of YPF identified with Network Analyzer and CytosHubba.

Network Analyzer			CytosHubba	
Rank	Target names	Betweenness centrality	Rank	Target names
1	CASP3	0.1855011	1	RELA ^a
2	TP53	0.17087517	2	TNF ^a
3	PIK3R1	0.14026847	3	IL4
4	PTGS2	0.13862876	4	IL6 ^a
5	TNF ^a	0.12369826	5	CXCL8
6	RELA ^a	0.11866108	6	IL2
7	MAPK1	0.11649041	7	CCL2
8	MAPK8 ^a	0.11517212	8	MAPK14 ^a
9	IL6 ^a	0.11309099	9	MAPK8 ^a
10	MAPK14 ^a	0.08753791	10	LCK

a: RELA, TNF, IL6, MAPK14 and MAPK8 were identified as the key targets by network analysis as well as by CytosHubba analysis.

Table 6
Hub target details of three key active components.

Compound No.	Compound names	Numbers of bound hub targets	Hub targets ^a
P3	wogonin	4	RELA, TNF, IL6, MAPK14
P13	astragaloside IV	2	MAPK8, MAPK14
M17	5-O-methylvisamminol (hydroxylation)	1	MAPK14

a: Hub targets of components shared with approved drugs for COVID-19.

important ingredient in YPF which has been studied thoroughly by many researchers for its anti-viral, anti-oxidant, anti-cancerous and anti-inflammatory activities (Wang, Li, Li, & Wang, 2017; Wu

et al., 2019). It regulated the production of inflammatory cytokines, including IL-6, TNF- α and GM-CSF (Li et al., 2017), and is the main active ingredients of Chinese medicines for the management of COVID-19 by inhibiting inflammatory mediators, regulating immunity, and eliminating free radicals through COX-2, CASP3, IL-6, MAPK1, MAPK14, MAPK8, and REAL in the signaling pathways of IL-17, arachidonic acid, HIF-1, NF- κ B, Ras, and TNF (Huang et al., 2020), which are consistent with our study.

It was found that the second-important component astragaloside IV may possess good efficacy on COVID-19. Astragaloside IV is one of the major and main active substances of *Astragali Radix*, demonstrated potential cardioprotective and immunological enhancement activities through experimentation *in vitro* and *in vivo*. It appeared to have powerful antagonistic effects on inflammatory, via regulating IL-1 β , TNF- α , ICAM and chemokine (Li, Hou, Xu, Liu, & Tu, 2017; Ren, Zhang, Mu, Sun, & Liu, 2013). 5-O-

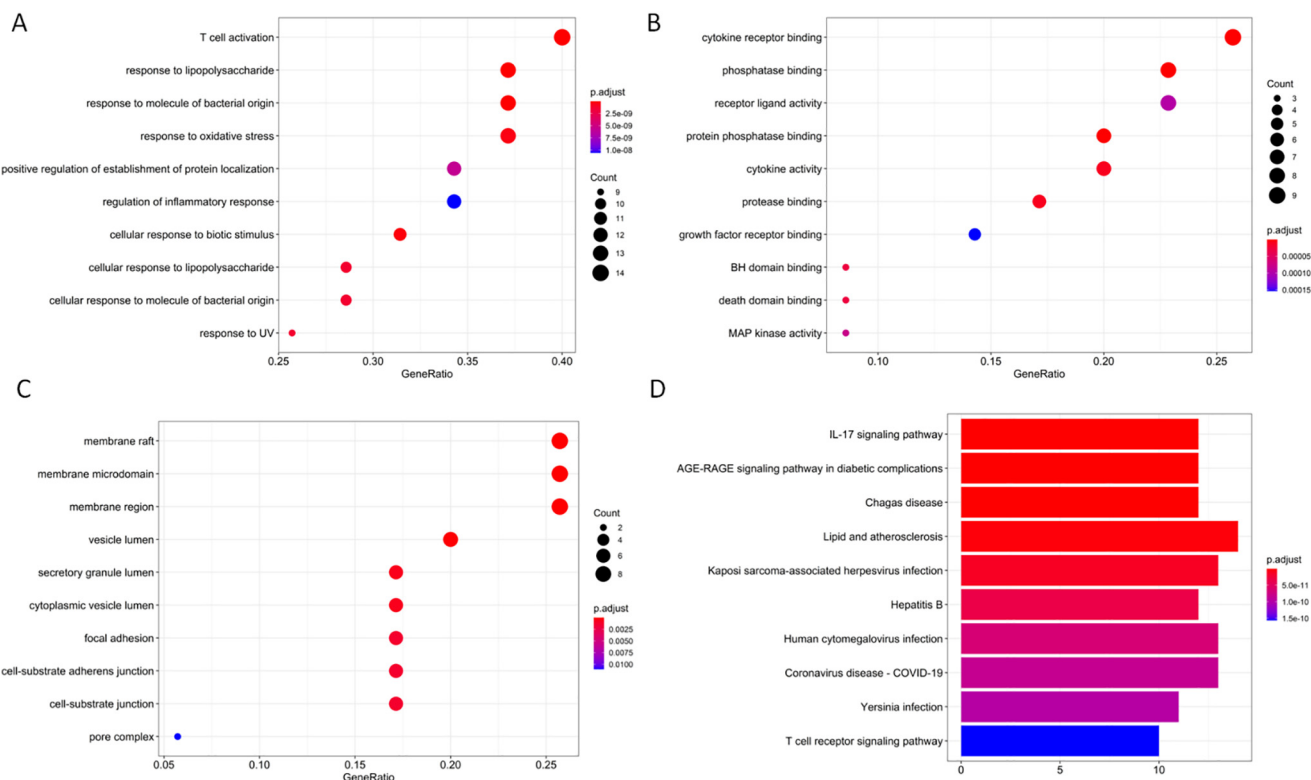


Fig. 9. GO analysis and KEGG pathways analysis by DAVID and STRING databases. GO analysis of candidate targets. The database showed the four remarkably enriched items in biological processes (BP, A), molecular function (MF, B), cell component (CC, C) and KEGG pathways of target genes (D).

methylvisamminol (3' hydroxylation), without relevant studies, may act on MAPK14 according to our study, and have effects on COVID-19. Even so, the targets could be further analyzed and validated to deeply understand the mechanism of 5-O-methylvisamminol (3' hydroxylation).

The results of network pharmacology and PPI analysis showed that the top targets involved RELA, TNF, IL-6, MAPK14 and MAPK8, which are the potential targets of the compounds of YPF. Elevated levels of tumor necrosis factor (TNF), a key pro-inflammatory cytokine, have been shown to be associated with increased COVID-19 mortality. In addition, anti-TNF therapies have a well-demonstrated ability to reduce inflammation and specifically reduce levels of pro-inflammatory cytokines associated with poor COVID-19 outcomes (Robinson et al., 2020). IL-6 was proven to be a key driver of the inflammation associated with COVID-19 infection (Zhou et al., 2020). As such, it has been hypothesized that monoclonal antibodies blocking IL-6 could help improve clinical outcomes in COVID-19 patients with severe pneumonia.

GO and KEGG pathway analysis further showed that the most important of YPF were T cell activation, response to molecule of bacterial origin, cytokine receptor binding, receptor ligand activity, cytokine activity, IL-17 signaling pathway, Chagas disease, lipid and atherosclerosis. This result indicated that these pathways might be critical biological processes through which YPF achieves its therapeutic effect. Therefore, we speculated that the multiple active compounds in YPF may play an important role in COVID-19 therapy by multiple signal pathways.

Though some results have been attained in this research, there are still limitations. The absorbable constituents of YPF were not identified thoroughly, and the targets of components should be further investigated to prove the speculation.

5. Conclusion

In this study, 61 components of YPF and 36 absorbable constituents were identified through UPLC-Q/TOF-MS, and five absorbable bioactive constituents were shown by network pharmacology analysis to have potential anti-COVID-19 effects. The major metabolic reactions of the absorbed constituents were demethylation, hydroxylation, sulfation and glucuronidation. All in all, the results clearly presented the metabolic pathways of YPF *in vivo* that not only provided the absorbable constituents but also, and more importantly, discovered potential targets and biological processing mechanisms of YPF, which will open up a new approach in the study of YPF in future.

Author Contributions

Participated in research design: Wang Linyan, Wang Bo. Conducted experiments: Wang Linyan, Zhang Lizong, Fang Mingsun, Guan Yang. Performed data analysis: Wang Linyan, Du Zhongyan, Pei Yanling. Wrote or contributed to the writing of the manuscript: Wang Linyan, Wang Bo, Guan Yang.

Declaration of Competing Interest

The authors declare that they have no known competing financial interests or personal relationships that could have appeared to influence the work reported in this paper.

Acknowledgements

The research was supported by the Natural Science Foundation of Zhejiang Province (No. LQ20H270008) and Natural Science Foundation of Zhejiang Chinese Medical University (No. 2018ZZ13).

Appendix A. Supplementary data

Supplementary data to this article can be found online at <https://doi.org/10.1016/j.chmed.2022.02.001>.

References

- Arrell, D. K., Zlatkovic, J., Kane, G. C., Yamada, S., & Terzic, A. (2009). ATP-sensitive K⁺ channel knockout induces cardiac proteome remodeling predictive of heart disease susceptibility. *Journal of Proteome Research*, 8, 4823–4834.
- Chen, J., Wang, W. Q., Shi, C. Y., & Fang, J. G. (2020). Thoughts on prevention and treatment of coronavirus disease 2019 (COVID-19) by traditional Chinese medicine. *Chinese Traditional and Herbal Drugs*, 51(5), 1106–1112.
- Du, H., Hou, X., Miao, Y., Huang, B., & Liu, D. (2020). Traditional Chinese Medicine: An effective treatment for 2019 novel coronavirus pneumonia (NCP). *Chinese Journal of Natural Medicines*, 18(3), 206–210.
- Gfeller, D., Michielin, O., & Zoete, V. (2013). Shaping the interaction landscape of bioactive molecules. *Bioinformatics*, 29(23), 3073–3079.
- Han, Z., Wang, X., Xu, M., Wang, Y., Yang, L., & Han, M. (2016). Optimization of supercritical fluid extraction and rapid resolution LC-MS/ESI identification of chromones from *Saposhnikovia Radix* through orthogonal array design. *Chinese Herbal Medicines*, 8(4), 314–322.
- Huang, Y. F., Bai, C., He, F., Xie, Y., & Zhou, H. (2020). Review on the potential action mechanisms of Chinese medicines in treating Coronavirus Disease 2019 (COVID-19). *Pharmacological Research*, 158, 104939–104977.
- Jia, M., Xiong, Y., Xue, Y., Wang, Y., & Yan, C. (2017). Using UPLC-MS/MS for characterization of active components in extracts of Yupingfeng and application to a comparative pharmacokinetic study in rat plasma after oral administration. *Molecules*, 22(5), 810–824.
- Li, H., Chen, X., Yang, Y., Huang, H. M., Zhang, L., Zhang, X., ... Li, J. (2017a). Wogonin attenuates inflammation by activating PPAR-gamma in alcoholic liver disease. *International Immunopharmacology*, 50, 95–106.
- Li, L., Hou, X., Xu, R., Liu, C., & Tu, M. (2017b). Research review on the pharmacological effects of astragaloside IV. *Fundamental & Clinical Pharmacology*, 31(1), 17–36.
- Li, L., Li, D., Xu, L., Zhao, P., Deng, Z., Mo, X., ... Gao, J. (2014). Total extract of Yupingfeng attenuates bleomycin-induced pulmonary fibrosis in rats. *Phytomedicine*, 22(1), 111–119.
- Li, X., Yang, H., Xiao, J., Zhang, J., Zhang, J., Liu, M., ... Ma, L. (2020). Network pharmacology based investigation into the bioactive compounds and molecular mechanisms of *Schisandrae Chinensis Fructus* against drug-induced liver injury. *Bioorganic Chemistry*, 96, 103553–103560.
- Li, Y., Zhao, L., Zhang, H., Jia, J., Lv, L., Zhou, G., ... Zhang, G. (2012). Comparative pharmacokinetics of prim-O-glucosylcimifugin and cimifugin by liquid chromatography-mass spectrometry after oral administration of *Radix Saposhnikovia* extract, cimifugin monomer solution and prim-O-glucosylcimifugin monomer solution to rats. *Biomedical Chromatography*, 26(10), 1234–1240.
- Li, Y., Zheng, B., Tian, H., Xu, X., Sun, Y., Mei, Q., ... Liu, L. (2017c). Yupingfeng Powder relieves the immune suppression induced by dexamethasone in mice. *Journal of Ethnopharmacology*, 200, 117–123.
- Liu, X., Ouyang, S., Yu, B., Liu, Y., Huang, K., Gong, J., ... Jiang, H. (2010). PharmMapper server: A web server for potential drug target identification using pharmacophore mapping approach. *Nucleic Acids Research*, 38(Web Server issue), W609–W614.
- Liu, X., Shen, J., Fan, D., Qiu, X., Guo, Q., Zheng, K., ... He, X. (2017). Yupingfeng San inhibits NLRP3 inflammasome to attenuate the inflammatory response in asthma mice. *Frontiers in Pharmacology*, 8, 944–955.
- Luo, H., Tang, Q. L., Shang, Y. X., Liang, S. B., Yang, M., Robinson, N., & Liu, J. P. (2020). Can Chinese medicine be used for prevention of corona virus disease 2019 (COVID-19)? A review of historical classics, research evidence and current prevention programs. *Chinese Journal of Integrative Medicine*, 26(4), 243–250.
- Ma, J., Zheng, J., Zhong, N., Bai, C., Wang, H., Du, J., ... Chen, P. (2018). Effects of YuPingFeng granules on acute exacerbations of COPD: A randomized, placebo-controlled study. *International Journal of Chronic Obstructive Pulmonary Disease*, 13, 3107–3114.
- Nikles, S., Monschein, M., Zou, H., Liu, Y., He, X., Fan, D., ... Bauer, R. (2017). Metabolic profiling of the traditional Chinese medicine formulation Yu Ping Feng San for the identification of constituents relevant for effects on expression of TNF-alpha, IFN-gamma, IL-1beta and IL-4 in U937 cells. *Journal of Pharmaceutical and Biomedical Analysis*, 145, 219–229.
- Oh, H. A., Choi, H. J., Kim, N. J., & Kim, D. H. (2014). Anti-stress effect of astragaloside IV in immobilized mice. *Journal of Ethnopharmacology*, 153(3), 928–932.
- Ren, S., Zhang, H., Mu, Y. P., Sun, M. Y., & Liu, P. (2013). Pharmacological effects of Astragaloside IV: A literature review. *Journal of Traditional Chinese Medicine*, 33(3), 413–416.
- Robinson, P. C., Liew, D. F. L., Liew, J. W., Monaco, C., Richards, D., Shivakumar, S., ... Feldmann, M. (2020). The potential for repurposing anti-TNF as a therapy for the treatment of COVID-19. *Med*, 1(1), 90–102.
- Ru, J. L., Li, P., Wang, J. N., Zhou, W., Li, B. H., Huang, C., ... Yang, L. (2014). TCMSP: A database of systems pharmacology for drug discovery from herbal medicines. *Journal of Cheminformatics*, 6, 13–18.
- Shen, L., Chen, W., Zhang, B., Liu, L., & Cao, Y. (2019). Integrating network pharmacology and bioinformatics analysis to explore the mechanism of

- Yupingfengsan in treating lung adenocarcinoma. *European Journal of Integrative Medicine*, 100967–100975.
- Shi, J., Zheng, L., Lin, Z., Hou, C., Liu, W., Yan, T., ... Liu, Z. (2015). Study of pharmacokinetic profiles and characteristics of active components and their metabolites in rat plasma following oral administration of the water extract of *Astragal radix* using UPLC-MS/MS. *Journal of Ethnopharmacology*, 169, 183–194.
- Song, T., Hou, X., Yu, X., Wang, Z., Wang, R., Li, Y., ... Wang, J. (2016). Adjuvant treatment with Yupingfeng Formula for recurrent respiratory tract infections in children: A Meta-analysis of randomized controlled trials. *Phytotherapy Research*, 30(7), 1095–2004.
- Sun, W., Meng, K., Qi, C., Yang, X., Wang, Y., Fan, W., ... Liu, J. (2015). Immune-enhancing activity of polysaccharides isolated from *Atractylodis macrocephalae* Koidz. *Carbohydrate Polymers*, 126, 91–96.
- Von Mering, C., Huynen, M., Jaeggi, D., Schmidt, S., Bork, P., & Snel, B. (2003). STRING: A database of predicted functional associations between proteins. *Nucleic Acids Research*, 31(1), 258–261.
- Wang, J., Li, K., Li, Y., & Wang, Y. (2017a). Mediating macrophage immunity with wogonin in mice with vascular inflammation. *Molecular Medicine Reports*, 16(6), 8434–8440.
- Wang, S. X., Wang, Y., Lu, Y. B., Li, J. Y., Song, Y. J., Nyamgerelt, M., & Wang, X. X. (2020). Diagnosis and treatment of novel coronavirus pneumonia based on the theory of traditional Chinese medicine. *Journal of Integrative Medicine*, 18(4), 275–283.
- Wang, X., Pan, C., Gong, J., Liu, X., & Li, H. (2016a). Enhancing the enrichment of pharmacophore-based target prediction for the polypharmacological profiles of drugs. *Journal of Chemical Information and Modeling*, 56(6), 1175–1183.
- Wang, X., Shen, Y., Wang, S., Li, S., Zhang, W., Liu, X., ... Li, H. (2017b). PharmMapper 2017 update: A web server for potential drug target identification with a comprehensive target pharmacophore database. *Nucleic Acids Research*, 45(W1), W356–W360.
- Wang, Z., Cai, X., Pang, Z., Wang, D., Ye, J., Su, K., ... Hu, C. (2016b). Yupingfeng Pulvis regulates the balance of T cell subsets in asthma mice. *Evidence-based Complementary and Alternative Medicine*, 2016, 1–7.
- Wu, Y. H., Chuang, L. P., Yu, C. L., Wang, S. W., Chen, H. Y., & Chang, Y. L. (2019). Anticoagulant effect of wogonin against tissue factor expression. *European Journal of Pharmacology*, 859, 172517–172525.
- Xu, J., & Zhang, Y. (2020). Traditional Chinese medicine treatment of COVID-19. *Complementary Therapies in Clinical Practice*, 39, 1–2.
- Yan, L., Chen, X., Guo, J., Qi, L., Qian, Y., & Zhou, X. (2010). Prevention of hospital-acquired pneumonia with Yupingfeng Powder in patients with acute cerebral vascular diseases: A randomized controlled trial. *Zhong Xi Yi Jie He Xue Bao*, 8(1), 25–29.
- Yang, J., Jiang, H., Dai, H., Wang, Z., Jia, G., & Meng, X. (2017). Feeble antipyretic, analgesic, and anti-inflammatory activities were found with regular dose 4'-O- β -D-glucosyl-5-O-methylvisamminol, One of the conventional marker compounds for quality evaluation of *Radix Saposhnikovia*. *Pharmacognosy Magazine*, 13(49), 168–174.
- Yang, Y., Islam, M. S., Wang, J., Li, Y., & Chen, X. (2020). Traditional Chinese medicine in the treatment of patients infected with 2019-new coronavirus (SARS-CoV-2): A review and perspective. *International Journal of Biological Sciences*, 16(10), 1708–1717.
- Ye, M., Luo, G., Ye, D., She, M., Sun, N., Lu, Y. J., & Zheng, J. (2020). Network pharmacology, molecular docking integrated surface plasmon resonance technology reveals the mechanism of Toujie Quwen Granules against coronavirus disease 2019 pneumonia. *Phytomedicine*, 85, 153401–153422.
- Yin, F. Q., Lan, R. X., Wu, Z. M., Wang, Z. J., Wu, H. H., Li, Z. M., ... Li, H. (2019). Yupingfeng polysaccharides enhances growth performance in Qingyuan partridge chicken by up-regulating the mRNA expression of SGLT1, GLUT2 and GLUT5. *Veterinary Medicine and Science*, 5(3), 451–461.
- You, Y., Yan, H., Wang, S., Luo, X., & Zhao, X. (2020). Therapeutic strategy of traditional Chinese medicine for COVID-19. *Drug Evaluation Research*, 43(4), 613–618.
- Zhai, J., Ren, Z., Wang, Y., Han, M., Han, N., Liu, Z., ... Yin, J. (2020). Traditional Chinese patent medicine Zhixiong Capsule (ZXC) alleviated formed atherosclerotic plaque in rat thoracic artery and the mechanism investigation including blood-dissolved-component-based network pharmacology analysis and biochemical validation. *Journal of Ethnopharmacology*, 254, 112523–112533.
- Zhang, D., Zhang, B., Lv, J. T., Sa, R. N., Zhang, X. M., & Lin, Z. J. (2020). The clinical benefits of Chinese patent medicines against COVID-19 based on current evidence. *Pharmacological Research*, 157, 1–21.
- Zhao, X., Sun, W., Zhang, S., Meng, G., Qi, C., Fan, W., ... Liu, J. (2016). The immune adjuvant response of polysaccharides from *Atractylodis macrocephalae* Koidz in chickens vaccinated against Newcastle disease (ND). *Carbohydrate Polymers*, 141, 190–196.
- Zhou, F., Yu, T., Du, R. H., Fan, G. H., Liu, Y., Liu, Z. B., ... Cao, B. (2020). Clinical course and risk factors for mortality of adult inpatients with COVID-19 in Wuhan, China: A retrospective cohort study. *The Lancet*, 395(10229), 1054–1062.
- Zuo, H., Zhang, Q., Su, S., Chen, Q., Yang, F., & Hu, Y. (2018). A network pharmacology-based approach to analyse potential targets of traditional herbal formulas: An example of Yu Ping Feng decoction. *Scientific Reports*, 8(1), 11418–11432.